Digitally Assisted Analog Front-end Power Management Strategy via Dynamic Reconfigurability for Robust Heart Rate Monitoring

Chengzhi Zong[1], Somok Mondal[2], Drew A. Hall[2], Roozbeh Jafari[1]

[1]Department of Electrical Engineering, University of Texas at Dallas
[2]Department of Electrical and Computer Engineering, University of California, San Diego
chengzhi.zong@utdallas.edu, somondal@eng.ucsd.edu, drewhall@ucsd.edu, rjafari@utdallas.edu

ABSTRACT

This paper presents a reconfiguration methodology to digitally assist a reconfigurable analog front-end (AFE), with the objective of reducing the power consumption of an ECG-based cardiac activity monitoring system, while maintaining an acceptable performance for the desired signal processing. In this study, we focus on the performance of ECG-based heart rate estimation as an example to demonstrate our proposed strategy. Utilizing the consistency and quasi-periodicity of the ECG waveform, two regions are pre-defined based on the prediction of the R peak by a normalized least mean square (NLMS) adaptive filter. The power consumption and performance of the AFE is dynamically reconfigured accordingly. Experimental evaluations show the system can measure heart rate variability (HRV) with an error of 0.5-4 beats/min with the sampling rate reduced from 488 sps to 100 sps and 40 sps for the two regions respectively, bit resolution reduced from 10-bit to 6-bit and noise tolerance substantially relaxed, offering an estimated 62% total power saving.

Keywords

Reconfigurable analog front end; electrocardiograph; heart rate variability; digital assistance; heart rate monitoring.

1. INTRODUCTION

The demand for enabling new applications to manage health-care and wellness has substantially increased in recent years. Among physiological signals, cardiac activity monitoring is one of the most important aspects of health monitoring systems because heart diseases can severely and suddenly threaten human life. Furthermore, the unpredictable nature of heart malfunctions requires long-lasting, uninterrupted monitoring, necessitating power efficient and wearable heart activity monitoring devices.

For the purpose of heart disease monitoring and analysis, monitoring heart rate, and in particular heart rate variability (HRV), has shown to be an important predictor for several heart diseases in the early stage [1]. Among existing methods for heart rate monitoring, the electrocardiogram (ECG), which involves capturing the electrical activities of the heart, is considered superior to other candidates due to its well-defined and informative waveforms [2].

Fig. 1 shows the architecture of the proposed bio-signal acquisition system. Generally, the parameters associated with an AFE, such as the sampling rate, ADC resolution, and noise performance are fixed and set for the worst case scenario at the design stage. Hence such designs are not optimal in terms of power efficiency. However, the recent advent of various reconfigurable analog circuitry [3, 4] suggest that sensor interface circuitry can be developed where one could reconfigure various circuit functionality and performance parameters based on the application requirements. Further, utilizing the well-established notion of digital assistance for analog circuits [5], a DSP back-end could provide appropriate feedback to a reconfigurable AFE in order to switch into any desired operation mode. In other words, with the usage of digital assistance for reconfigurable analog circuits, one can leverage the fact that the signal acquisition quality can be compromised to lower the power consumption of the AFE while maintaining satisfactory performance of the signal processing algorithms. This will be demonstrated and established through the results presented in this paper.

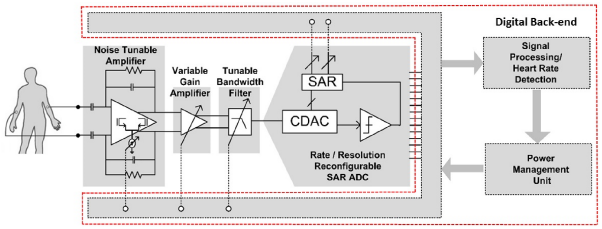

Figure. 1. A digitally-assisted reconfigurable ECG acquisition system.

Some of the relevant existing techniques have explored various sampling techniques [6-8]. A state-of-the-art ECG front-end [6] employed derivative-based adaptive sampling where based on a switched capacitor differentiator different sampling rates were applied to high and low activity ECG regions respectively. A level-crossing sampling for ECG acquisition was adopted in [7]. However, such sampling techniques are potentially susceptible to noise, interference, artifacts, etc. Compressive sensing based AFEs generally perform well when the incoming signals are sparse [8], however, our approach does not require the sparsity on the incoming signals and can realize signal processing in conjunction with adaptive sensing (e.g., heart rate detection in our case study) while the compressive sensing will only compress the incoming signals. In this work, two activity based regions are robustly defined as in [6] using an alternative proposed DSP technique based on prediction of the next upcoming R peak. The precise digital feedback using our proposed strategy would allow a dynamic reconfiguration to accurately capture only the QRS region on-the-fly. Further, since this technique is not driven by analog circuitry, the window width can also be adjusted to cover extra margin around the high-activity QRS region, if required.

2. SIGNAL PROCESSING

It is well known that the QRS complex is the most distinguishable component of the ECG waveform for reliable heart rate estimation. Therefore, configuring the AFE in a higher power and sensitivity mode only for the region that contains QRS complex while ignoring the remaining area will effectively lower the power consumption of the AFE. Particularly, if an assumption is made that the heart rate itself or its changing trend remains largely consistent over a short-time window, a predictor could be applied to forecast the position of upcoming QRS complex based on the previous detected positions. Generally, cardiac activity has a finite, but small, HRV. To account for which, a corresponding small time margin could be added around the predicted position to capture the so-called *R-peak region* and perform an accurate search for R peak. This three phase strategy involving an upcoming R peak prediction, window definition to capture the *R-peak region* and the actual R peak identification has been illustrated in Fig. 2.

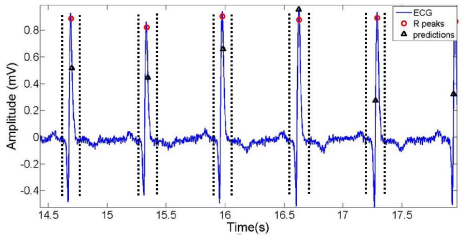

Figure 2. Dynamic region definition based on R peak prediction shown over captured ECG

However, to account for large and sudden HRV, the above strategy would require a larger time margin, or equivalently an enlarged *R-peak region,* implying using the higher power mode for longer duration, diminishing the low-power benefits of prediction. Therefore, to maintain the power efficiency and acceptable performance, instead of brutally enlarging *R-peak region*, we limited the range of *R-peak region* based on the presumed HRV constraints and apply a relatively less accurate, but also less sample-intensive, autocorrelation method to operate upon the downsampled data from the *R-peak region* and scanty data from the remaining *non-R-peak region.*

2.1 R-peak Prediction

In order to predict the *R-peak* and *non-R-peak regions*, a normalized least mean square (NLMS) based adaptive filter is implemented as shown in (1-4),

$$y(n) = X(n)^T W(n) \tag{1}$$

$$e(n) = d(n) - y(n) \tag{2}$$

$$W(n+1) = W(n) + 2\mu(n)e(n)X(n) \tag{3}$$

$$\mu(n) = \mu/(2X(n)^T X(n) + \varepsilon) \tag{4}$$

where $X(n)$ is the column vector of previous N R-R intervals at time n (R peak is detected by the CWT-based algorithm presented below), $W(n)$ is the column vector of N coefficients for the prediction model at time n, and N is the order of the adaptive filter, here N is chosen to be 5 with an assumption that the most recent 5 R-R intervals contribute mostly to the prediction for the upcoming one. The error $e(n)$ between the predicted value $y(n)$ and true value $d(n)$ is then used along with the normalized updating step size $\mu(n)$ to update the coefficients vector from $W(n)$ to $W(n+1)$. It may be noted that this R-R interval prediction process needs to be repeated iteratively. In this work, all initial adaptive filter coefficients $W(n)$ are set to $1/N$ and eventually converge after a few heart beats. Further, at start-up, the AFE may be deployed at the highest sensitivity (and power consumption) mode to guarantee error-free initial inputs to this predictor.

2.2 Heart Rate Estimation Algorithm

2.2.1 R-peak region – wavelet based R peak detection: The continuous wavelet transform (CWT) constructs a time-frequency representation of the ECG signal and transforms the time-domain into the wavelet-domain, as indicated in (5).

$$T(a,b) = \frac{1}{\sqrt{a}} \int_{-\infty}^{+\infty} x(t)\psi^*\left(\frac{t-b}{a}\right)dt \tag{5}$$

The scale factor a is selected to allow establishing correlations between the mother wavelet $\psi(t)$ and the R peak of the ECG signal $x(t)$, and used together with the thresholding method in the wavelet domain to determine the R peaks [9]. The performance of this method is accurate and robust and the degradation mostly only results from introducing extra noise/artifacts with much higher amplitude or an R peak-like impulse signal. Therefore, being highly resistant to quantization noise and input-referred noise, the adoption of CWT algorithm not only yields an accurate R peak detection but also could relax the requirement of the resolution of ADC and input-referred noise of amplifier in the AFE, which makes itself a suitable candidate for the estimation of heart rate in the R-peak region.

2.2.2 Non-R-peak region – autocorrelation based estimation: Another alternative method for heart rate estimation is based on the autocorrelation function (ACF) to search for the fundamental frequency of heart rate. Compared with wavelet-based algorithms, this method does not rely solely on capturing a predefined segment of the signal (e.g., R peak) with high sensitivity but potentially on the entire period of the signal captured with lower sensitivity. Therefore, the use of this algorithm theoretically will require less power consumption for the ECG front-end in comparison to the wavelet-based algorithm and can provide coarse heart rate estimation, which is validated in the next section. Particularly when the actual HRV exceeds the presumed constraint, i.e., the R peak lies outside the R-peak region, this ACF based estimation could still provide acceptable heart rate tracking performance.

3. EVALUATION AND DISCUSSION

3.1 Tradeoff between Performance & Power

The ECG data used in this paper was collected using a customized bio-signal acquisition board [10], which includes a TI ADS1299 analog front end and an MSP430 microcontroller.

By fixing the sampling rate at 488 sps, which is around the suggested rate for ECG sensing [2], we evaluated the impact of varying ADC resolution on the wavelet-based heart rate estimation performance for different noise tolerance levels. In our simulations, the noise tolerance level was measured by calculating the signal-to-noise ratio (SNR) after artificially introducing white Gaussian noise to the captured data. Referring to [6], we selected the input dynamic range for the ADC to be ±5mV and assumed appropriate gain to satisfy the same by applying proper scaling to the ADS1299 data. Our results in Fig. 3 show the performance of

the wavelet-based heart rate estimation remains highly accurate (error ≈ 0.1 beats/min) when the resolution is equal to or larger than 6-bit while degrading sharply lower than 6-bit. Therefore, for the wavelet-based algorithm, the lower bound of the resolution is set to be 6-bit as the starting point to continue to evaluate the impact of sampling rate. In Fig. 4, we gradually reduced the sampling rate to test its impact on the wavelet-based performance for various SNR values. The results show that the heart rate tracking error remains fairly small (error < 0.5 beats/min) for sampling rate larger than or equal to 100 sps, but increases sharply with sampling rate below this boundary, which may be due to the fact that the power of the most distinguishable frequencies for R peak is largely reduced [9].

In Fig. 5 and 6, we performed the similar test on the impact of sampling rate, ADC resolution, and noise tolerance for the autocorrelation-based heart rate estimation. The results show that the best performance (around ±2 beats/min) is worse than that of the wavelet-based algorithm (around ±0.1 beats/min), but the performance degradation over the tunable parameters, especially for sampling rate, has a much lower slope than that of the wavelet-based algorithm. This phenomenon experimentally confirms our choice of the autocorrelation-based estimation method over the wavelet-based algorithm for the non-R-peak region, since the wavelet-based algorithm is not able to provide acceptable performance in an ultra-low power configuration when the tunable parameters are aggressively adjusted as the autocorrelation-based algorithm does.

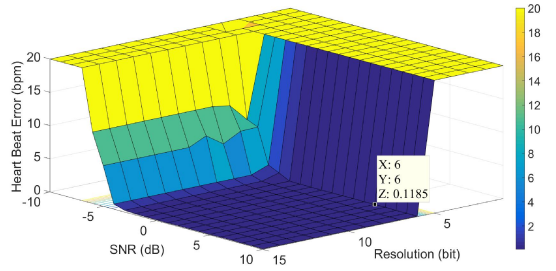

Figure 3. Wavelet-based heart rate estimation error over different resolution and SNR, with sampling rate = 488 sps.

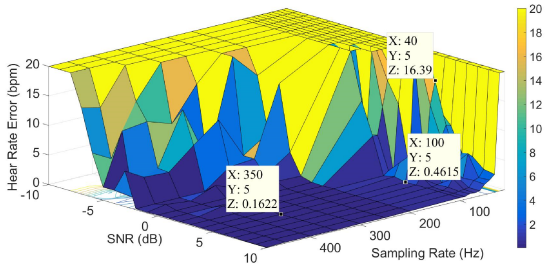

Figure 4. Wavelet-based heart rate estimation error over different sampling rate and SNR, with resolution = 6-bit

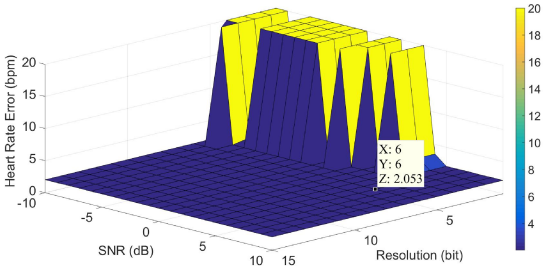

Figure 5. Autocorrelation-based heart rate estimation error over different resolution and SNR, with sampling rate = 488 sps.

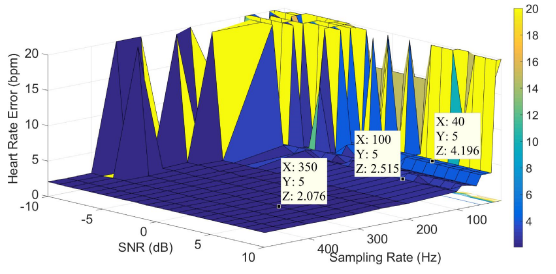

Figure 6. Autocorrelation-based heart rate estimation error over different sampling rate and SNR, with resolution = 6-bit.

3.2 Power Management: Analysis & Estimate

The proposed power management scheme involves dynamic reconfiguration between three different power modes while simultaneously maintaining acceptable heart rate estimation performance. Our results have indicated that three AFE parameters viz. resolution, sampling rate and noise performance can be significantly relaxed to allow power savings via dynamic reconfiguration. Table I summarizes these AFE parameters corresponding to the modes indicated in Fig. 7, which constitutes our dynamic AFE reconfiguration strategy. The reconfigured parameters corresponding to Mode-b and Mode-c have been defined based on sample application acceptable heart-rate error and using experimental results with trade-off analyses presented in previous sections. The performance error constraints are set to 0.5 and 4 beats/min for wavelet and autocorrelation-based approaches, respectively.

3.2.1 Power Estimate: The two major components in a typical AFE are the ADC and the amplifier. Preliminary SPECTRE simulations of a reconfigurable rate/resolution SAR ADC have indicated satisfactory power scaling achievable as indicated in Table-I. Simulations of a current tunable chopper-stabilized biopotential amplifier consuming power of 87.1nW and 44.5nW exhibit noise levels of $110nV/\sqrt{Hz}$ and $235nV/\sqrt{Hz}$ respecively indicating that noise can also be satisfactorily traded with power. The power-consuming components in DSP are the CWT and ACF blocks, which primarily comprise multiply-accumulate operations (MAC). On one hand, the power consumption of CWT equals to:

$$P_{CWT} = N * S_1 * W_1 * P_{MAC} \quad (6)$$

Where N, S_1, W_1 and P_{MAC} are number of wavelet scales, sampling rate, width of mother wavelet function in unit of samples and power of one MAC operation. When the Mexican hat wavelet is chosen and wavelet center frequency set to 16Hz and 17Hz as

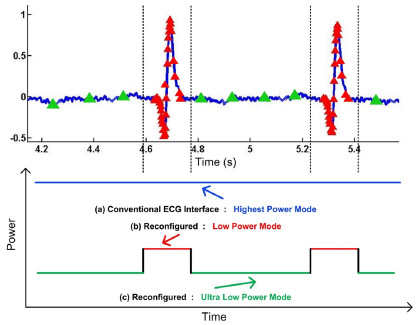

Figure 7. Reconfigurable modes illustrated over captured ECG.

Table I. AFE Dynamic Reconfigurability

MODE	(a)	(b)	(c)
Sampling rate	**High** 488 sps	**Moderate** 100 sps	**Low** 40 sps
Resolution	**High** 10-bit	**Low** 6-bit	**Low** 6-bit
Noise Tolerance	**Low**	**High** SNR 3 dB	**High** SNR 3 dB
Error	0.1 bpm	0.5 bpm	4 bpm
Estimated ADC power	32.3nW	3.41nW	2.74nW
Estimated Amplifier Power	87.1nW	44.5nW	44.5nW
Estimated DSP power	8.40μW	205.9nW	50.7nW

suggested in [9], W_1 equals to $4S_1/17$. On the other hand, the power of ACF equals to:

$$P_{ACF} = \frac{(2*T*S_2 - lag)*(lag+1)}{2*T} * P_{MAC} \quad (7)$$

where S_2, T and lag corresponds to the sampling rate, window length in seconds and time lag range in samples for the autocorrelation in each window. To account for the heart rate between 40 and 180 beats/min, lag is set to $7S_2/6$ and T is set to 3 seconds. One thing to note is the autocorrelation needs to be running continuously in both Mode-b (after downsampling) and Mode-c. The estimate energy are 75pJ and 33pJ for 10-bit and 6-bit MAC operations through the PrimeTime simulation with TSMC 0.18μm technology, Vdd=1.1V and clock frequency=10kHz. Therefore, with S_1 set to 488 sps and 100 sps for Mode-a and Mode-b respectively and S_2 set to 40 sps for Mode-c as indicated in Table I, the estimate of DSP power for Mode-a (CWT), Mode-b (CWT+ACF) and Mode-c (ACF) are 8.40μW, 205.9nW and 50.7nW, respectively.

3.2.2 Power Savings Analysis: The total power of AFE and DSP for our proposed scheme could be estimated by:

$$P_{total} = \frac{P_a * t_a + P_b * t_b + P_c * t_c}{t_a + t_b + t_c} \quad (8)$$

where P_a, P_b, P_c are the total AFE plus DSP power for three modes as indicated in Table I, and t_a, t_b, t_c are obtained from the predictor to represent the time duration for the three modes. We performed a simulation on the 10-min ECG data. With time margin around predicted R peak equal to 0.4 second, the estimated power saving switching from Mode-a to our proposed scheme is more than 95% due to the dominance of DSP power in Mode-a, with the error increased from 0.1 bpm to 1.5 bpm. Practically, downsampling the signal in Mode-a to the same sampling rate as Mode-b before applying CWT would largely reduce the DSP power for Mode-a, which still yields a potential 62% power saving when proposed scheme is applied. The overhead introduced by this power management strategy is the prediction scheme which requires a simple logic circuit to check for the transitioning conditions from one mode to another using two simple counters. This incurs a negligible overhead compared to the power consumption of the signal acquisition and processing.

4. CONCLUSIONS

In this paper, a signal processing centered control strategy for AFE reconfiguration was presented. A prominent advantage of the proposed strategy includes creation of predictive cues on when the AFE must be activated or sent to the low power modes (e.g., lowering the sampling frequency or ADC resolution). This is achieved by predicting future *R-peak regions* using an NLMS adaptive filter. Another important feature of the proposed strategy lies within the algorithmic aspect of robust heart rate estimation, which is achieved by employing two different rate estimation algorithms. The effectiveness of these two algorithms has been established through preliminary experimental evaluations. In addition, potential power saving is also discussed and analyzed along with the simulation-based power estimate.

5. ACKNOWLEDGMENT

This work was supported in part by the National Science Foundation under grant CNS-1150079. Any opinions, findings, conclusions, or recommendations expressed in this material are those of the authors and do not necessarily reflect the views of the funding organizations.

6. REFERENCES

[1] M. Chessa, G. Butera, G. A. Lanza, E. Bossone, A. Delogu, G. De Rosa, G. Marietti, L. Rosti, and M. Carminati, "Role of heart rate variability in the early diagnosis of diabetic autonomic neuropathy in children," *Herz*, vol. 27, no. 8, pp. 785–790, 2002.

[2] M. Raju, "Heart rate and EKG monitor using the MSP430fg439," *Texas Instruments, Dallas, Texas, USA*, 2005.

[3] M. Yip and A. P. Chandrakasan, "A resolution-reconfigurable 5-to-10-bit 0.4-to-1 v power scalable SAR ADC for sensor applications," 2013.

[4] S. O'Driscoll, K. V. Shenoy, and T. H. Meng, "Adaptive resolution ADC array for an implantable neural sensor," *Biomedical Circuits and Systems, IEEE Transactions on*, vol. 5, no. 2, pp. 120–130, 2011.

[5] B. Murmann and B. Boser, "Digitally assisted analog integrated circuits," *Queue*, vol. 2, no. 1, p. 64, 2004.

[6] R. F. Yazicioglu, S. Kim, T. Torfs, H. Kim, and C. Van Hoof, "A 30 w analog signal processor ASIC for portable biopotential signal monitoring," *Solid-State Circuits, IEEE Journal of*, vol. 46, no. 1, pp. 209–223, 2011.

[7] Y. Hong, I. Rajendran, and Y. Lian, "A new ECG signal processing scheme for low-power wearable ECG devices," in *Microelectronics and Electronics (PrimeAsia), 2011 Asia Pacific Conference on Postgraduate Research in*, pp. 74–77, IEEE, 2011.

[8] D. Gangopadhyay, E. G. Allstot, A. M. Dixon, K. Natarajan, S. Gupta, and D. J. Allstot, "Compressed sensing analog front-end for bio-sensor applications," *Solid-State Circuits, IEEE Journal of*, vol. 49, no. 2, pp. 426–438, 2014.

[9] I. R. Legarreta, P. S. Addison, M. Reed, N. Grubb, G. R. Clegg, C. E. Robertson, and J. N. Watson, "Continuous wavelet transform modulus maxima analysis of the electrocardiogram: beat characterization and beat-to-beat measurement," *International Journal of Wavelets, Multiresolution and Information Processing*, vol. 3, no. 01, pp. 19–42, 2005.

[10] V. Nathan, J. Wu, C. Zong, Y. Zou, O. Dehzangi, M. Reagor, and R. Jafari, "Demonstration paper: A 16-channel Bluetooth enabled wearable EEG platform with dry-contact electrodes for brain computer interface," in *ACM International Conference on Wireless Health*, 2013.